Research Paper

CD163-Macrophages Are Involved in Rhabdomyolysis-Induced Kidney Injury and May Be Detected by MRI with Targeted Gold-Coated Iron Oxide Nanoparticles

Alfonso Rubio-Navarro[1*], Mónica Carril[2,3*], Daniel Padro[2], Melanie Guerrero-Hue[1], Carlos Tarín[1], Rafael Samaniego[4], Pablo Cannata[5], Ainhoa Cano[2], Juan Manuel Amaro Villalobos[1], Ángel Manuel Sevillano[6], Claudia Yuste[6], Eduardo Gutiérrez[6], Manuel Praga[6], Jesús Egido[1,7], Juan Antonio Moreno[1✉]

1. Renal, Vascular and Diabetes Research Lab. Fundación Instituto de Investigaciones Sanitarias-Fundación Jiménez Díaz, Autónoma University. Av. Reyes Católicos 2, 28040, Madrid, Spain.
2. CIC biomaGUNE. Paseo Miramón, 182, 20009, San Sebastián, Spain.
3. Ikerbasque, Basque Foundation for Science, 48011, Bilbao, Spain.
4. Confocal Microscopy Unit, IIS-Gregorio Marañón, C/ Doctor Esquerdo, 46 28007 Madrid, Spain.
5. Pathology Department, Fundación Instituto de Investigaciones Sanitarias-Fundación Jiménez Díaz, Autónoma University. Av. Reyes Católicos 2, 28040, Madrid, Spain.
6. Department of Nephrology, 12 de Octubre Hospital, 28041 Madrid, Spain
7. Centre of Biomedical Research in network of Diabetes and Metabolic disease associated (CIBERDEM).

* Both authors contributed equally.

✉ Corresponding author: Juan Antonio Moreno, PhD, Vascular, Renal and Diabetes Research. Fundación Instituto de Investigaciones Sanitarias-Fundación Jiménez Díaz. Av. Reyes Católicos 2, 28040-Madrid. Spain. Email: jamoreno@fjd.es.

Abstract

Macrophages play an important role in rhabdomyolysis-acute kidney injury (AKI), although the molecular mechanisms involved in macrophage differentiation are poorly understood. We analyzed the expression and regulation of CD163, a membrane receptor mainly expressed by anti-inflammatory M2 macrophages, in rhabdomyolysis-AKI and developed targeted probes for its specific detection *in vivo* by MRI. Intramuscular injection of glycerol in mice promoted an early inflammatory response, with elevated proportion of M1 macrophages, and partial differentiation towards a M2 phenotype in later stages, where increased CD163 expression was observed. Immunohistological studies confirmed the presence of CD163-macrophages in human rhabdomyolysis-AKI. In cultured macrophages, myoglobin upregulated CD163 expression *via* HO-1/IL-10 axis. Moreover, we developed gold-coated iron oxide nanoparticles vectorized with an anti-CD163 antibody that specifically targeted CD163 in kidneys from glycerol-injected mice, as determined by MRI studies, and confirmed by electron microscopy and immunological analysis. Our findings are the first to demonstrate that CD163 is present in both human and experimental rhabdomyolysis-induced AKI, suggesting an important role of this molecule in this pathological condition. Therefore, the use of probes targeting CD163-macrophages by MRI may provide important information about the cellular composition of renal lesion in rhabdomyolysis.

Key words: rhabdomyolysis, CD163, macrophages, gold coated iron oxide nanoparticles, MRI, acute kidney injury.

Introduction

Acute kidney injury (AKI) is a frequent complication of rhabdomyolysis, with an estimated incidence of 10-50% (1, 2), increasing the mortality rate of these patients (3). Rhabdomyolysis is produced by the breakdown of the skeletal muscle, resulting in myoglobin release into the circulation (1). Myoglobin is filtered through the glomeruli and reabsorbed in the proximal tubules. Myoglobin and its

heme-derived products play a key role in rhabdomyolysis-induced renal damage by increasing apoptosis of proximal tubular cells and promoting vasoconstriction, oxidative stress, pro-inflammatory chemokines secretion and nitric oxide consumption (4-6).

Recent studies suggest that rhabdomyolysis-induced AKI could be an inflammatory disease, where macrophages play an important role in the pathogenesis of the renal lesions (7, 8). Different macrophage subsets, namely M1 (classically activated and proinflammatory) and M2 (anti-inflammatory and tissue-remodeling functions) participate in the development of renal disorders, including rhabdomyolysis (9, 10). However, the molecular mechanisms involved in macrophage differentiation in rhabdomyoysis are not known. The hemoglobin scavenger receptor CD163 is mainly expressed by M2 macrophages at sites of inflammation. CD163 presents important immunoregulatory properties, by inducing anti-inflammatory IL-10 release and heme oxygenase-1 (HO-1) synthesis (11). Under oxidant conditions, filtered myoglobin dissociates into heme and globin. HO-1 transforms heme to biliverdin, a reaction that produces carbon monoxide and iron, which is subsequently stored in ferritin (12). Therefore, the CD163/HO-1/ferritin system decreases cellular exposure to heme-derived products (13, 14). We previously reported CD163-expressing macrophages in kidneys from patients reporting renal accumulation of hemoglobin-derived heme, such as haematuric glomerulonephritis (14, 15) and hemolytic disorders (16). However, whether CD163 may be involved in rhabdomyolysis-induced kidney injury has not been previously analyzed. Heme, similar to hemoglobin, has been demonstrated to induce CD163 expression (17). High heme levels have been reported in rhabdomyolysis as consequence of both direct myoglobin dissociation and heme-release from cytochromes and other heme-containing proteins that are released as consequence of tubular cell death in this condition. Therefore, we hypothesized that myoglobin-derived heme may promote macrophage differentiation towards a CD163 like-M2 phenotype to resolve rhabdomyolysis associated renal damage.

Magnetic resonance imaging (MRI) is widely used for early lesion detection in a number of diseases because of its good spatial resolution and average contrast agent sensitivity. This non-invasive diagnostic tool has been effectively used in the clinic for the diagnosis of kidney disease. Determination of macrophage infiltrate may provide relevant information about disease status and progression. Thus, targeting of macrophages (usually total population or M1 fraction) has been pursued in preclinical imaging of several diseases by MRI, either by passive labeling or by active targeting of membrane receptors with vectorized nanoprobes (18-21). Tracking of macrophage infiltration by MRI has been employed in models of kidney transplantation, fibrosis and ischemia-reperfusion (22-26). Recent studies have been designed to detect M1/M2 macrophage polarization by MRI in animal models (27, 28). CD163 may be an interesting target to determine disease-associated macrophages by MRI studies because of its specific expression pattern and its utility as a diagnostic biomarker of macrophage activation in inflammatory diseases (29). The design of MRI probes for targeted imaging based on nanoparticles is currently a very active field of research (30). In particular, gold-coated iron oxide nanoparticles vectorized with antibodies have been successfully used as T_2 contrast agents in the targeting of different types of cells (31-33), including CD163-macrophages (34). In the present article, we analyzed the expression of CD163 (both in human kidney biopsies and a mouse model of rhabdomyolysis-induced AKI), the molecular mechanisms involved in its regulation, and whether gold-coated iron oxide nanoparticles may be suitable for the *in vivo* detection of CD163-macrophages in this pathological condition by a non-invasive way.

Results

Glycerol-administration induced renal dysfunction and oxidative stress *in vivo*.

Intramuscular injection of glycerol in mice led to a rise in BUN and serum creatinine as compared with controls, peaking at 24h and decreasing at day 7 after glycerol injection (**Figure 1A-B**). Urinary myoglobin concentration was also elevated from day 1 to 3, reflecting the glycerol-mediated breakdown of the skeletal muscle (**Figure 1C**). Comparable with the decline of renal function in the first 72h, histological analysis reported severe kidney injury in glycerol-treated mice, characterized by interstitial edema, and extensive tubular damage with focal loss of brush border, intratubular debris, cast formation and apoptotic tubular cells (**Figure 1D, Supplemental Figure 1**). TUNEL staining confirmed the presence of tubular cell apoptosis, mainly at 24h after glycerol administration (**Figure 1D-E**). Increased mRNA expression of the tubular injury biomarkers Kim-1 and Ngal was observed after glycerol administration (**Figure 1F-G**). All these findings were consistent with the differences in renal function.
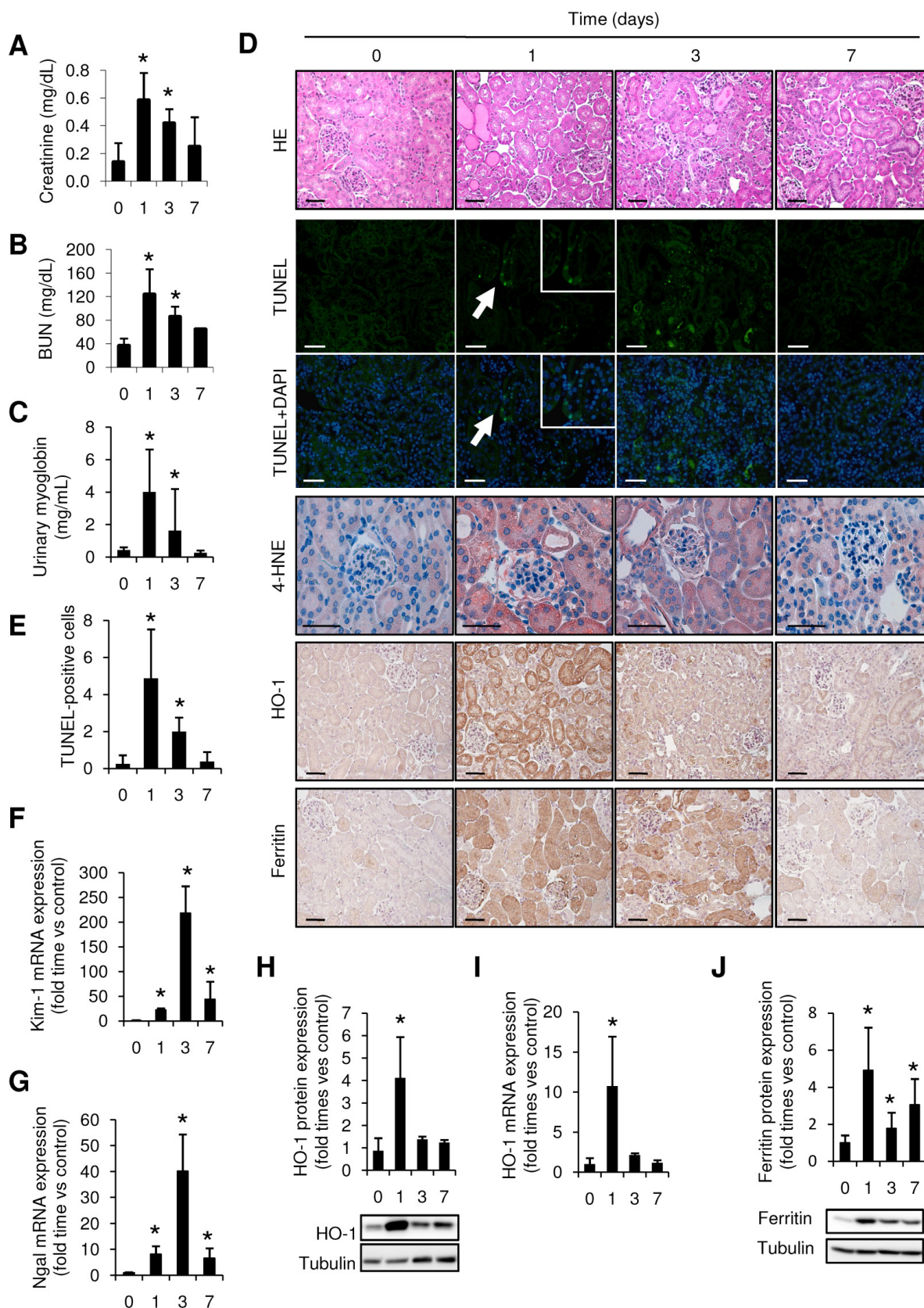
Figure 1. Rhabdomyolysis promotes renal damage by oxidative stress and tubular apoptosis. C57Bl/6 mice (males, 12 weeks old) were injected with saline or 10 ml/kg 50% glycerol in each thigh caudal muscle. Creatinine (**A**), BUN (**B**) and urinary myoglobin (**C**) were elevated from day 1 to 3, decreasing at day 7. (**D**) Representative images showing hematoxylin and eosin staining, confocal TUNEL images, and immunhistochemical 4-HNE, HO-1 and Ferritin images of mouse kidneys, scale bar 50 μM. (**E**) Quantitative TUNEL positive cells analysis in mice with rhabdomyolysis. Expression of tubular injury biomarkers Kim-1 (**F**) and Ngal (**G**), as determined by real time RT-PCR, in kidneys from mice with rhabdomyolysis. HO-1 expression, as determined by western-blot (**H**) and RT-PCR (**I**) was elevated 24h after glycerol-injection; whereas ferritin presence was increased from day 1 to day 7, as determined by Western-blot (**J**). Mice (n=5) per day-group. Results are expressed as mean ± SE. * $p < 0.05$ vs non-treated mice.

Rhabdomyolysis has been previously associated to oxidative stress (35), so we analyzed the presence of the oxidative markers 4-HNE and HO-1 in our model. Administration of glycerol promoted mRNA and protein expression of HO-1, reaching a maximum value at 24h after glycerol administration **(Figure 1 H-I)**. Similar results were obtained when we determined the presence of 4-HNE, confirming the presence of oxidative stress **(Figure 1D)**. Increased ferritin protein expression was also reported in glycerol-treated mice, indicating an increased heme-catabolism and further iron accumulation in the kidneys from these mice (**Figure 1J**).

CD163 was increased in both experimental and human rhabdomyolysis-AKI.

An increased inflammatory response, characterized by augmented CCL2, CCL5, IFN-γ and TNF-α mRNA expression, was observed after glycerol-administration (mainly at 24h and 72h post-injection, and decreasing at day 7) (**Figure 2A**). Immunohistochemical analysis of cross-sections showed an increased and sustained accumulation of interstitial F4/80-macrophage infiltrate (**Figure 2B**). To examine the macrophage phenotype associated to glycerol-induced rhabdomyolysis, we determined the renal expression of Arg2 and Arg1 isoforms, associated to classical activated M1 and alternative M2 macrophages, respectively. Western-blot and real-time PCR analysis of Arg2 and Arg1 revealed simultaneous expression of M1 and M2 markers in kidneys from 3 days after glycerol-injection, comparable with the increased accumulation of macrophage infiltrate (F4/80) (**Figure 2B-D**). Arg2 (M1) was most abundantly expressed at day 3, whereas Arg1 (M2) increased progressively from day 3 to 7. Indeed, calculation of M2/M1 ratio demonstrated the dominance of M2 over the M1 macrophage phenotype at day 7 (**Figure 2E**). In line with these results, CD163 positive macrophages (M2-like macrophages) were mainly found 7 days after glycerol administration (**Figure 2B**). Inmunohistological analysis in consecutive renal sections showed co-localization of the M2-marker CD206 (mannose receptor) with CD163 positive cells (arrows in **Figure 2F**). Moreover, gene expression analysis in kidney tissue confirmed the higher mRNA expression of CD163, mannose receptor and anti-inflammatory cytokines IL-4 and IL-10, at this late time point (**Figure 2A and C**). These results indicate that glycerol-induced rhabdomyolysis promotes an early inflammatory response, with elevated proportion of M1 macrophages, and a partial differentiation towards a M2 phenotype in later stages, where increased CD163 is observed.

In order to validate whether CD163 is also expressed in human rhabdomyolysis-induced AKI, we performed immunohistological studies in a kidney biopsy from a 73-year-old patient that was admitted at our hospital for rhabdomyolysis-associated AKI following long time immobile posture caused by a traumatism (creatine kinase 43,938 U/L, Creatinine 10.36 mg/dL) (**Figure 3A**). Histological analysis of the renal biopsy reported the presence of acute tubular damage, with tubules showing dilatation and flattening of the epithelial cells and containing brown granular material and protein casts, as well as interstitial CD68-macrophage infiltrate (**Figure 3B**). Importantly, we also found CD163 positive macrophages, mainly associated with CD68-macrophages, as confirmed by dual confocal immunofluorescence (**Figure 3C**). Neither CD68 nor CD163-positive macrophages were observed in healthy renal tissue (**Figure 3B**). Finally, our results show that the major part of CD163 positive macrophages also expressed CD206 and CD163L1 (M2 markers) in human rhabdomyolsysis.

Myoglobin promoted CD163 expression through HO-1 and IL-10 induction.

To gain insight into the molecular mechanisms of CD163 upregulation in rhabdomyolysis, we incubated macrophages isolated from the mouse peritoneal cavity with clinically relevant myoglobin concentrations (0-2.5 mg/mL) for 48h in presence or absence of the HO-1 inducer CoPP (Cobalt protoporphyrin) and an IL-10 blocking antibody. As reported in **Figure 4**, myoglobin promoted HO-1 and IL-10 mRNA expression in a dose-dependent manner, peaking at 6h, and remaining elevated 48h later (**Figure 4A-B**). These results were confirmed by confocal microscopy, showing increased HO-1 protein expression in myoglobin treated cells (**Figure 4C**). In line with the mRNA results, myoglobin augmented IL-10 secretion in macrophages supernatants, and this effect was greater in cells pre-treated with CoPP, illustrating a positive effect of HO-1 activity on IL-10 release, as previously reported (36) (**Figure 4D**). In fact, CoPP enhanced myoglobin-mediated effect on both HO-1 and IL-10 mRNA expression (**Supplemental Figure 2A**). However IL-10 blockade did not modify myoglobin-mediated HO-1 mRNA expression (**Supplemental Figure 2B**). Importantly, myoglobin increased CD163 mRNA expression at 48h (**Figure 4E**). Since heme may result from renal myoglobin degradation in rhabdomyolysis, we also determined the effect of this molecule on CD163 expression. Similar to myoglobin, heme (equimolar concentrations) also induced CD163 expression in macrophages (**Figure 4F**). Interestingly, we observed

that pre-stimulation of HO-1 with CoPP augmented myoglobin-mediated CD163 expression, whereas the opposite effect was obtained with an IL-10 blocking antibody (**Figure 4F**). Moreover, we found a positive association between IL-10 and CD163 mRNA expression in kidneys from mice with rhabdomyolysis (r=0.45, p<0.05).
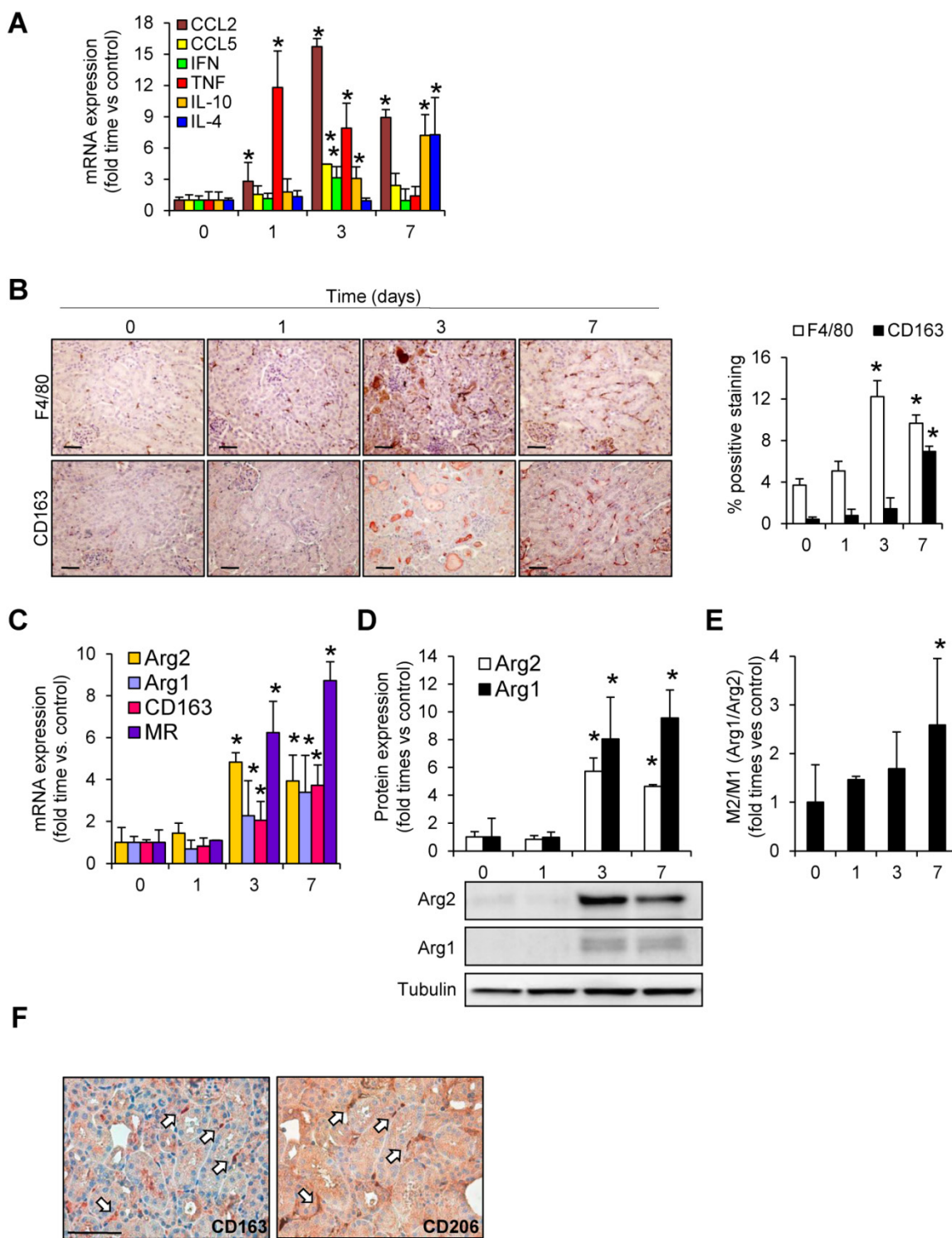
Figure 2. Rhabdomyolysis induces macrophages recruitment in murine kidneys. (**A**) Expression of pro-inflammatory (CCL2, CCL5, IFN-γ, TNF-α) and anti-inflammatory (IL-10 and IL-4) molecules, as determined by real time RT-PCR, in mice with rhabdomyolysis (**B**) Representative inmunohistochemistry (left panel) and semiquantitative assessment (right panel) of total infiltrating macrophages (F4/80) and CD163-macrophages in kidneys from mice with rhabdomyolysis, scale bar 50 μM. Expression of M1 (Arg2) and M2 (Arg1, CD163 and mannose receptor (MR)) macrophage markers, as determined by RT-PCR (**C**) and western-blot (**D**). Arg2 and Arg1 protein expression values were corrected by loading control (Tubulin) and expressed as M2/M1 ratio (**E**). Mice (n=5) per day-group. Results are expressed as mean ± SE. * p<0.05 vs non-treated mice. (**F**) Representative serial micrographs of CD206 and CD163, (white arrows indicate the presence of CD206 in CD163-macrophages), scale bar 50 μM.
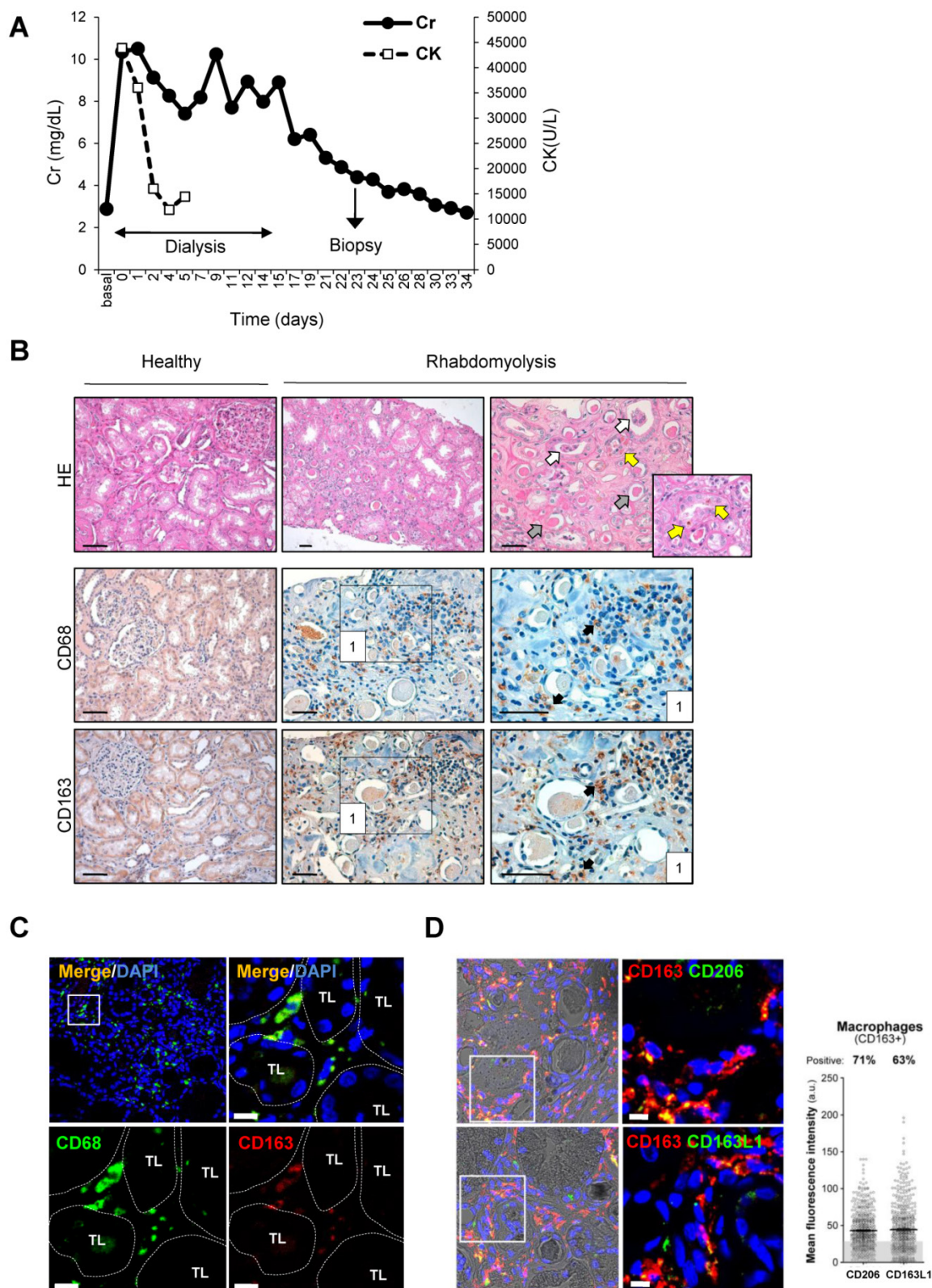
Figure 3. Rhabdomyolysis induces renal macrophages recruitment in a patient with rhabdomyolysis-induced AKI. (**A**) Creatinine (Cr) and creatine kinase (CK) serum levels indicated severe rhabdomyolysis-AKI in a 73-year-old patient that required dialysis for 14 days. Renal biopsy was performed on day 24. (**B**) Representative inmunohistochemistry showing hematoxylin and eosin staining (upper panel), total infiltrating macrophages (CD68, middle panel) and CD163-macrophages (CD163, lower panel) in the renal biopsy from with rhabdomyolysis-associated AKI, scale bar 50 µM. Healthy renal tissue was used as control. Histological analysis reported increased interstitial macrophage infiltration and the presence of acute tubular damage (white arrows), with tubules showing dilatation and flattening of the epithelial cells and containing brown granular material and protein casts (grey arrows), heme-iron deposits (yellow arrow). The rectangle shows the region of interest for which high-magnification images are shown in the right panels. (**C**) Representative confocal microscopy images showing co-localization of CD68 (green) and CD163 (red) in macrophages within kidney of the patient with rhabdomyolysis, scale bar 10 µM. Nuclei were stained with DAPI (blue). TL: tubular lumen. (**D**) Representative confocal microscopy images (left panel) and semiquantitative assessment (right panel), showing co-localization of CD206 (green), CD163L1 (green) and CD163 (red) in macrophages within kidney of the patient with rhabdomyolysis, scale bar 10 µM. Nuclei were stained with DAPI (blue).
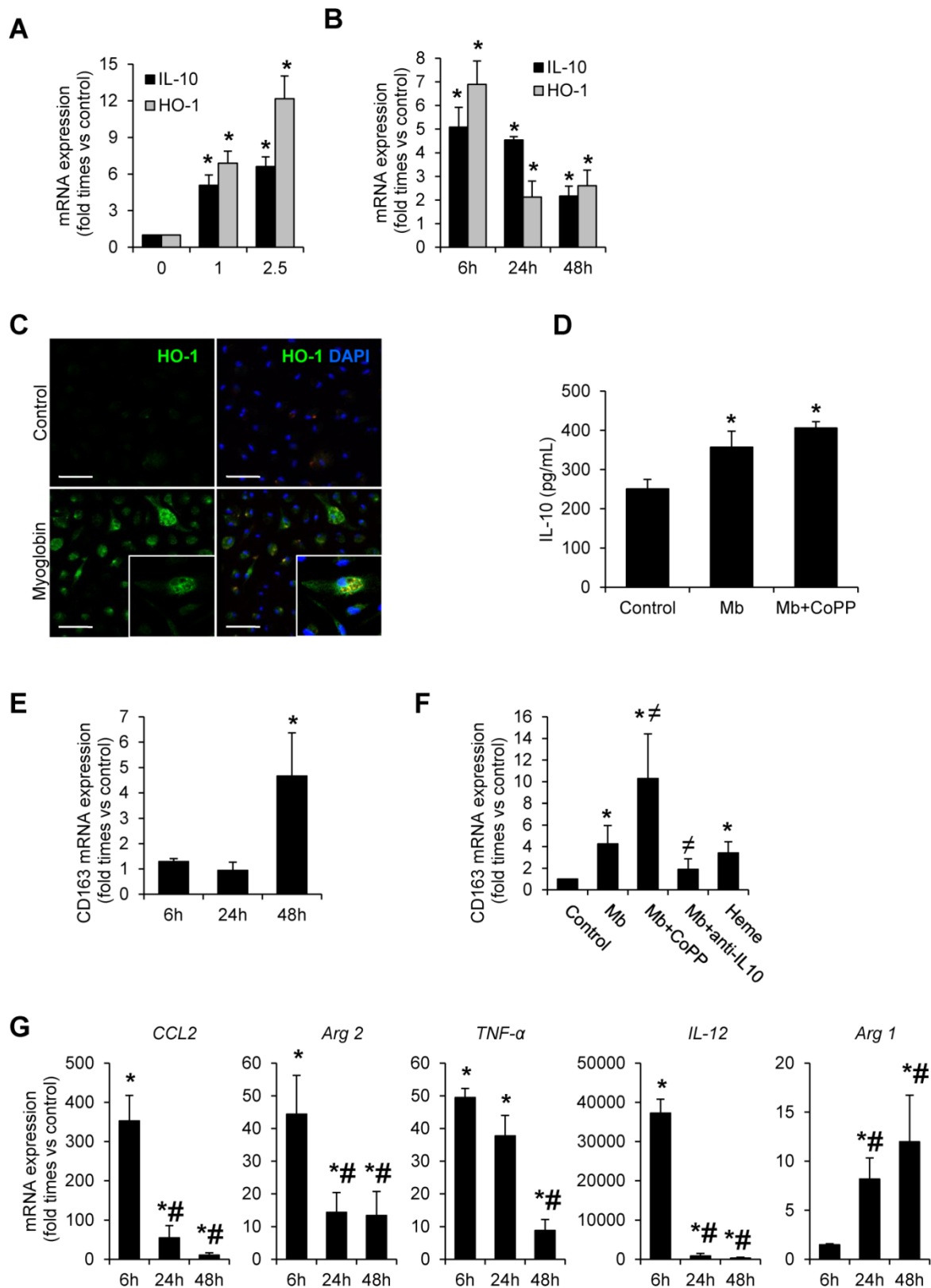
Figure 4. Myoglobin induces CD163 expression in mouse peritoneal macrophages through HO-1 and IL-10 induction. Macrophages were isolated from the mouse peritoneal cavity and treated with myoglobin (Mb) (0-2.5 mg/mL) for 48h. Dose- (**A**) and time-(**B**) enhanced mRNA expression of IL-10 and HO-1, as determined by real time RT-PCR, in myoglobin-treated macrophages. (**C**) Representative confocal microscopy images showing enhanced HO-1 expression in macrophages treated with myoglobin (1mg/mL) for 24h. Scale bar 50 μM (**D**) IL-10 release was determined by ELISA in cell supernatants. (**E-F**) Expression of CD163 in macrophages treated with myoglobin (1mg/mL) or equimolar concentration of heme (60μM) for 48h in presence or absence of the HO-1 inducer CoPP or an IL-10 blocking antibody (1μg/mL), as determined by RT-PCR. (**G**) Expression of M1 (CCL2, Arg2, TNF-α, IL-12) and M2 markers (Arg1) in macrophages stimulated with myoglobin (1mg/mL), as determined by RT-PCR. Results are expressed as mean±SE of at least three independent experiments. * p<0.05 as compared with non-treated cells, ≠ p< 0.05 as compared with cells stimulated with Mb, # p< 0.05 as compared with cells treated with Mb for 6 hours.

Quantitative real-time PCR analysis in myoglobin-treated cells reported a pro-inflammatory profile at 6h, characterized by an increase of expression of CCL2, Arg2, TNF-α and IL-12; however the expression of these M1 markers decreased progressively overtime. The opposite trend was observed for Arg1, a M2 marker (**Figure 4G**). Altogether, our results indicate that myoglobin promotes an early inflammatory M1 response and further M2-like differentiation at later stages, where CD163 expression is increased *via* HO-1/IL-10 pathway.

In vivo detection of CD163 by MRI in a mice model of rhabmodyolysis.

We have recently developed a highly sensitive targeted probe based on gold-coated iron oxide nanoparticles functionalized with antibodies against CD163 for the specific detection of CD163-expressing macrophages in atheromatous lesions (34); however, its utility in kidney disorders has not been previously analyzed. For that reason, once demonstrated the presence of CD163-macrophages in rhabdomyolysis kidney injury, we tested whether our nanoparticles may be useful for early identification of CD163-positive macrophages in this pathological condition. The full characterization of these nanoparticles, as superparamagnetic materials and contrast agents, has been previously described by our group (31-34). Briefly, UV-Vis spectra showed the characteristic gold plasmon resonance band in all nanoparticles after the gold coating process (**Figure 5A-C**). Gold and iron content in the nanoparticles was 59.3±0.8% and 4.03±0.05%, respectively, as obtained from ICP-OES analysis. Relaxivity measurements were performed at 7 T and room temperature resulting in r_2 and r_1 values of 157 mM^{-1}s^{-1} and 10 mM^{-1}s^{-1}, respectively. The specificity of our nanoparticles was confirmed in mouse peritoneal macrophages stimulated with dexamethasone, a CD163 inducer (37) (**Figure 5D**).

Next, we injected the nanoparticles (either NP-CD163 or NP-IgG) 3 days after rhabdomyolysis induction in both, control and glycerol-injected mice. Kidneys were imaged before nanoparticles injection and 48h post-injection. A significant signal intensity decrease over time was observed in kidneys from mice with rhabdomyolysis and injected with NP-CD163, with respect to the pre-injection signal ($p<0.05$), indicating an increased accumulation of CD163-targeted nanoparticles (**Figure 5E-G**). However, no significant variations in signal intensity were observed in mice with rhabdomyolysis and injected with the control probe (NP-IgG). Importantly, NP-CD163 injection did not decrease kidney signal intensity in control mice as compared to pre-injection signal, demonstrating the specificity of the NP-CD163 derived signal (**Figure 5E-G**). Electron microscopy analysis confirmed the presence of nanoparticles within interstitial macrophages in kidneys from mice with rhabdomyolysis and injected with NP-CD163, whereas no nanoparticles were found in the same mice injected with NP-IgG (**Figure 5H**).

To verify data obtained by MRI and electron microscopy, we analyzed the presence of CD163-positive macrophages in the kidneys from these mice. Administration of glycerol led to a significant ($p<0.05$) increase in BUN and serum creatinine in both NP-CD163- (92±45 mg/dL and 0.7±0.4 mg/dL, respectively) and NP-IgG-injected mice (108±87 mg/dL and 0.6±0.5 mg/dL, respectively), as compared with controls (22±4 mg/dL and 0.1±0.1 mg/dL, respectively). In line with these results, histological analysis of kidneys harvested after MRI scan showed typical rhabdomyolysis associated renal damage, characterized by the presence of interstitial edema, tubular dilatation, intratubular debris and inflammatory F4/80 macrophage infiltrate in glycerol-injected mice (either injected with NP-CD163 or NP-IgG), but not in controls (**Figure 6A-C**). Inmunohistological analysis in consecutive renal sections showed co-localization of F4/80-macrophages with CD163 positive cells (arrows in **Figures 6B**). As reported in **Figure 6A-C**, glycerol-injection increased the presence of CD163-positive macrophages in both mice injected with NP-CD163 or NP-IgG; however a low CD163-positive staining was reported in control mice. We also found a positive correlation between the presence of CD163-macrophages in kidneys and decrease in CNR intensity obtained by MRI (r=0.56, p=0.044). Real-time PCR analysis confirmed the increased mRNA expression of CD163 in mice with rhabdomyolysis (**Figure 6D**). Furthermore, we determined the renal expression of other macrophage markers in this experimental model. Western-blot and real-time PCR analysis showed not only enhanced Arg2 (M1) expression but also increased presence of Arg1 (M2) in kidneys from glycerol-injected mice treated with either NP-CD163 or NP-IgG (**Figure 6E-G**). On the other hand, no biochemical or histological renal alterations were observed in mice after NP-CD163 injection, indicating no toxic effects for these nanoparticles *in vivo*, in agreement with previous studies conducted with similar iron-oxide nanoparticles (31-34), (**Supplemental Figure 3 and Supplemental Table 1**).
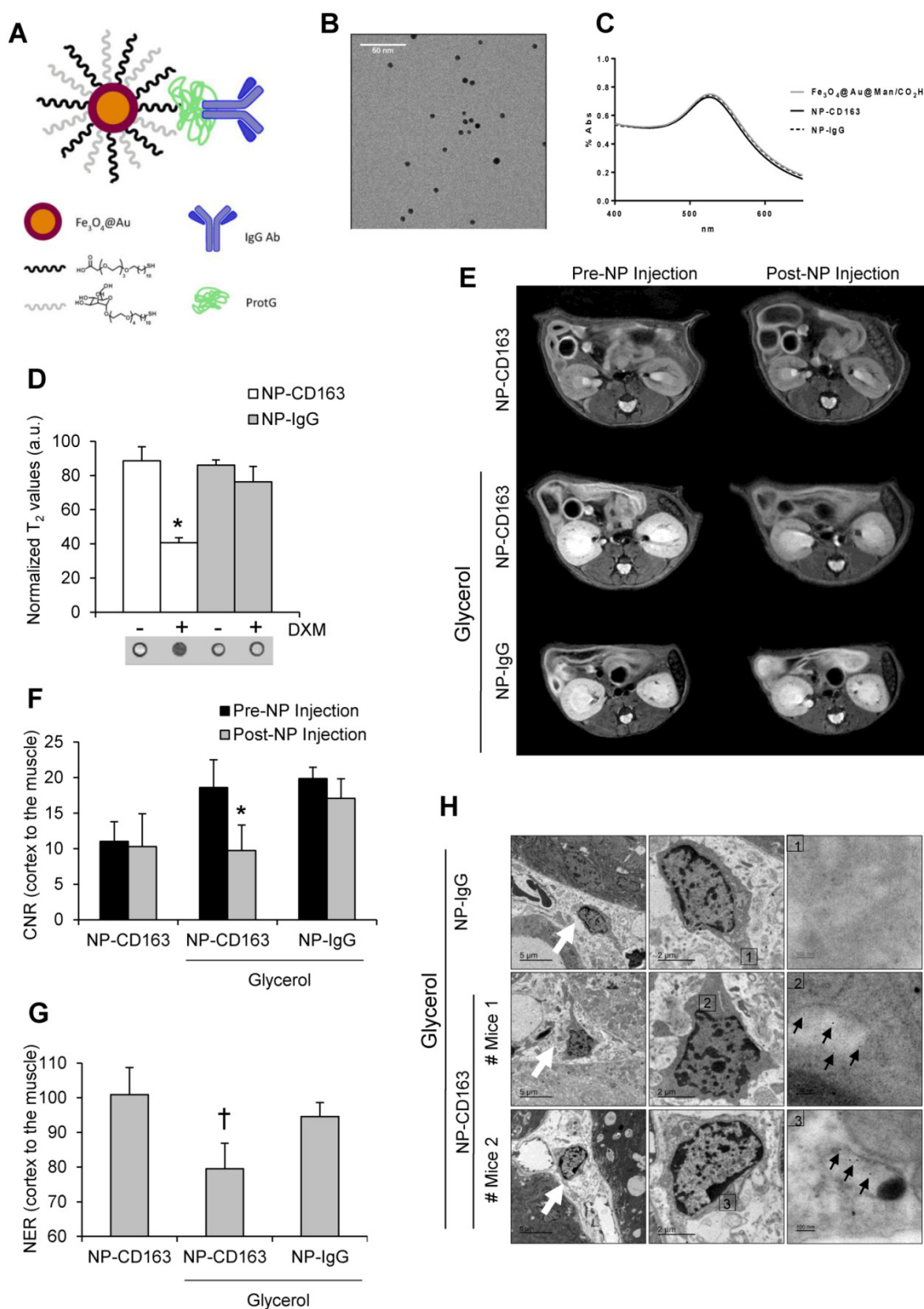
Figure 5. *In vivo* detection of CD163 by MRI in the glycerol model of rhabdomyolysis (**A**) Schematic representation of the nanoparticles administered in mice. Nanoparticles consisted of a gold-coated iron oxide core covered with thiol ligands bearing mannose and a carboxylic acid. ProtG was covalently linked through a peptide bond to the carboxylic moieties and anti-CD163 (NP-CD163) or IgG antibodies (NP-IgG) were subsequently grafted on them. (**B**) TEM micrograph of NP-CD163 and (**C**) UV-Vis spectra of gold-coated NPs before and after IgG antibodies conjugation. (**D**) Graph showing the normalized T_2 values obtained from MRI images of mouse peritoneal macrophages incubated with NP-CD163 or NP-IgG (as control) in presence of dexamethasone for 24h (DXM, a CD163 inducer). Mean±SD of 3 independent experiments. * $p<0.05$ vs. NP-CD163 without dexamethasone. The corresponding MRI phantoms are shown below the graph. (**E**) Representative magnetic resonance images obtained pre (0h) and post (48h) nanoparticles injection in mice with rhabdomyolysis. Graph showing the contrast-to-noise-ratio (CNR) of the kidney cortex with respect to muscle pre- and post-nanoparticle injection (**F**) and normalized-enhancement-ratio (NER) of the kidney cortex with respect to muscle 48 hours after nanoparticle injection (**G**) in mice with rhabdomyolysis and control. * $p<0.05$ vs pre-nanoparticle injection. † $p<0.05$ vs healthy mice or mice with rhabdomyolysis and injected with NP-IgG. (**H**) Detection of nanoparticles in mice by using TEM. Left panels shows 4000x magnification of renal cortex. White arrows show the presence of infiltrating macrophages in the kidney of mice 5 days after *i.m.* injection of glycerol. Central panel shows 12000 x magnification of macrophages. The rectangle shows the region of interest for which high-magnification images are shown in the right panels (120000 x magnification). Black arrows show the presence of nanoparticles in mice with rhabdomyolysis and injected with NP-CD163, but not in those mice treated with NP-IgG.
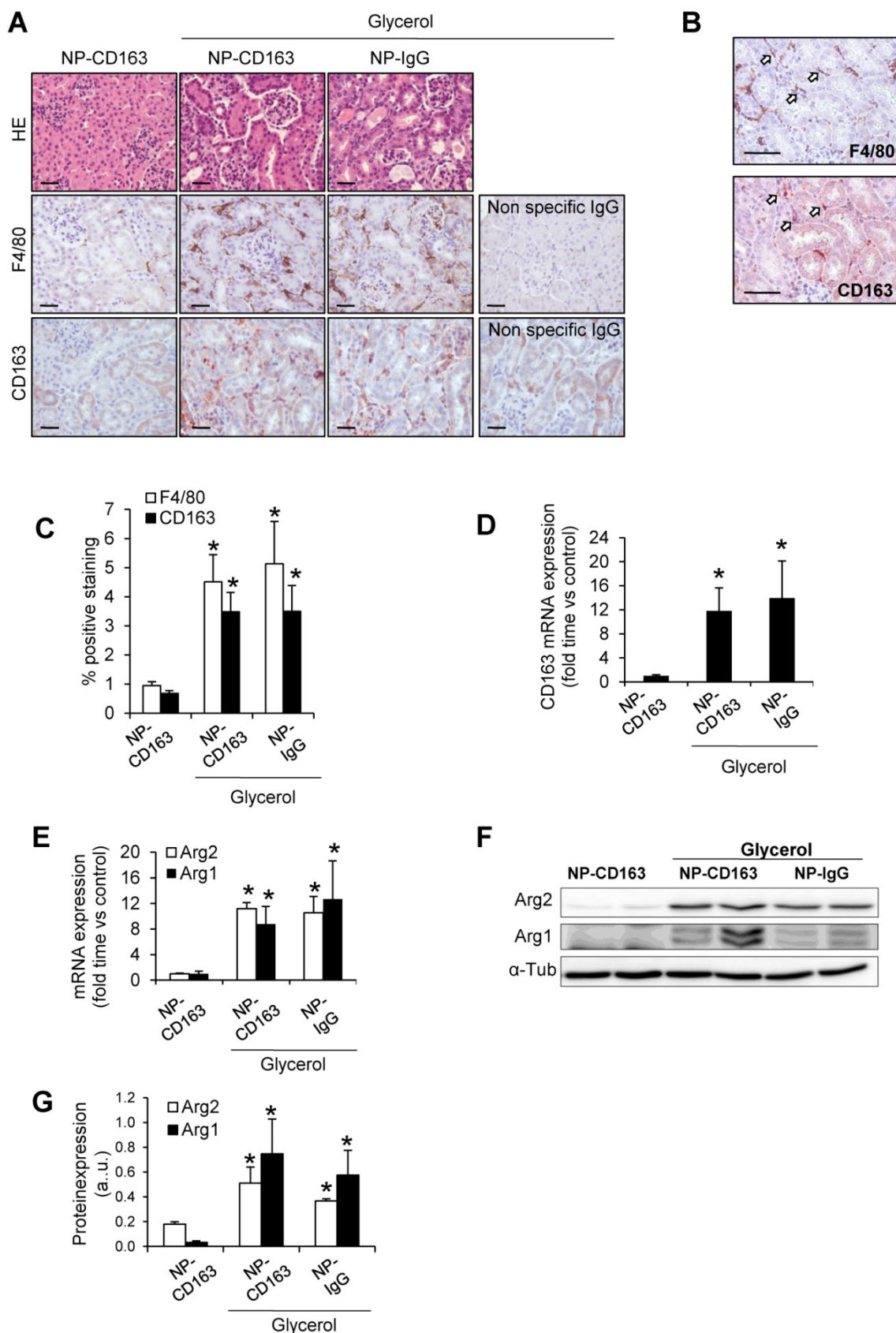
Figure 6. Validation of the presence of CD163 in kidneys harvested after imaging studies. (A) Representative images showing hematoxylin and eosin, total macrophages (F4/80) and CD163-macrophages in kidneys obtained from mice after imaging studies, scale bar 50 µM. (B) Representative serial micrographs of F4/80 and CD163 (white arrows indicate the presence of CD163 in CD68-macrophages), scale bar 50 µM. (C) Semiquantitative assessment of total infiltrating macrophages (F4/80) and CD163-positive staining and CD163 gene expression, as determined by RT-PCR (D). Expression of M1 (Arg2) and M2 (Arg1) macrophage markers, as determined by RT-PCR (E) and western-blot (F-G). Mice (n=5) per group. * p<0.05 vs non-treated mice.

Myoglobin-derived macrophages and fibrosis in rhabdomyolysis

Because of the role of macrophages in fibrosis, we determined fibrotic extracellular matrix and tested the changes in expression of genes involved in fibrosis in our experimental model (**Figure 7**). Glycerol-injected mice showed increased extracellular matrix deposition, mainly interstitial and perivascular, as determined by Sirius red staining (**Figure 7A-B**). In order to determine the molecular mechanism involved in rhabdomyolysis-mediated fibrosis we performed western blot and real-time-PCR in kidney homogenates. Western-blot and real time PCR analysis revealed that fibronectin, type I collagen, and alpha smooth muscle actin were main components of the fibrotic extracellular matrix in glycerol-injected mice (**Figure 7C-E**). Increased mRNA and protein expression of the pro-fibrotic mediator, TGF-β, was also elevated in rhabdomyolysis-mice (**Figure 7C-E**).

Since macrophage depletion reduced fibrosis in experimental rhabdomyolysis (8), we analyzed whether myoglobin may directly promote extracellular matrix production by macrophages. Our results showed that myoglobin-stimulated macrophages did not show significant increase in both fibronectin or type I collagen at mRNA level (**Figure 7F**). In the same line, no increased fibronectin or type I collagen secretion was observed in the cell supernatant upon exposure to myogobin (**Figure 7G**). We then asked whether the fibrogenic effects of macrophages may be driven *via* production of pro-fibrotic mediators, such as connective tissue growth factor (CTGF) or TGF-β. Real time PCR analysis revealed an increased mRNA expression of both CTGF and TGF-β in myoglobin-stimulated macrophages (**Figure 7H**). Contrary to macrophages, murine tubular epithelial cells showed increased mRNA expression and enhanced protein release of both fibronectin and type I collagen in presence of myoglobin, suggesting a key role of these cells in the fibrogenic response associated to rhabdomyolysis (**Figure 7I-J**). Altogether, our results may indicate that myoglobin-derived macrophages could contribute to fibrosis throughout production of fibrotic mediators (CTGF and TGF-β), therefore maintaining the synthesis of extracellular matrix proteins by tubular renal cells, which have a prominent fibrogenic role in this pathological condition.

Discussion

In the current study we demonstrate for the first time an increased renal mRNA and protein CD163 expression in a mouse model of rhabdomyolysis-induced AKI, which is characterized by increased oxidative stress, inflammatory infiltrate and tubular apoptosis. Moreover, we confirmed the presence of CD163-positive macrophages in a kidney biopsy from a patient with rhabdomyolysis-associated AKI. We observed that myoglobin promotes an early inflammatory M1 response and a partial differentiation towards a M2-skewed polarization phenotype at later stages, where increased CD163 expression is observed *via* HO-1 activation and further IL-10 release. In addition, these myoglobin-derived macrophages could contribute to fibrosis throughout the production of fibrotic mediators, such as CTGF and TGF-β, but no by increasing the synthesis of proteins of the extracellular matrix. Finally, we prepared gold-coated iron oxide nanoparticles vectorized with an anti-CD163 antibody and tested them for the specific detection of CD163 in rhabdomyolysis by MRI. Overall, our findings suggest a potentially important role of CD163 in the pathophysiology of rhabdomyolysis-associated renal damage, where the use of nanoparticles targeting CD163 may provide important information about kidney macrophage subtype distribution by a non-invasive way.

There are only a few published cases describing human the pathogenic mechanisms involved in human rhabdomyolysis-associated renal damage (8, 38). In the renal biopsy from a patient with severe rhabdomyolysis-AKI we observed increased CD68-macrophage infiltrate, similar to previous studies including patients with both infection- and drug-induced rhabdomyolysis (8, 38). In agreement with the results obtained in humans, increased F4/80 macrophage infiltrate has been reported after intramuscular glycerol-injection in mice, as we have observed in our study (39, 40). Inflammation is recognized as a contributor to renal damage in rhabdomyolysis. Thus, depletion of macrophages prevents renal dysfunction by decreasing apoptosis of tubular epithelial cells and reducing the expression of inflammatory mediators during experimental glycerol-induced AKI (41). In a recent study, macrophage depletion reduced histologic lesions, fibrosis and improved both kidney repair and mouse survival, suggesting a key role for macrophages in the progression of rhabdomyolysis-mediated renal damage (8). Our data strongly suggest that fibrotic effects of myoglobin-derived macrophages are not related to an enhanced synthesis of extracellular matrix proteins, but also to production of fibrotic mediators, such as CTGF and TGF-β, that could activate the fibrogenic response of tubular cells or fibroblasts (42).
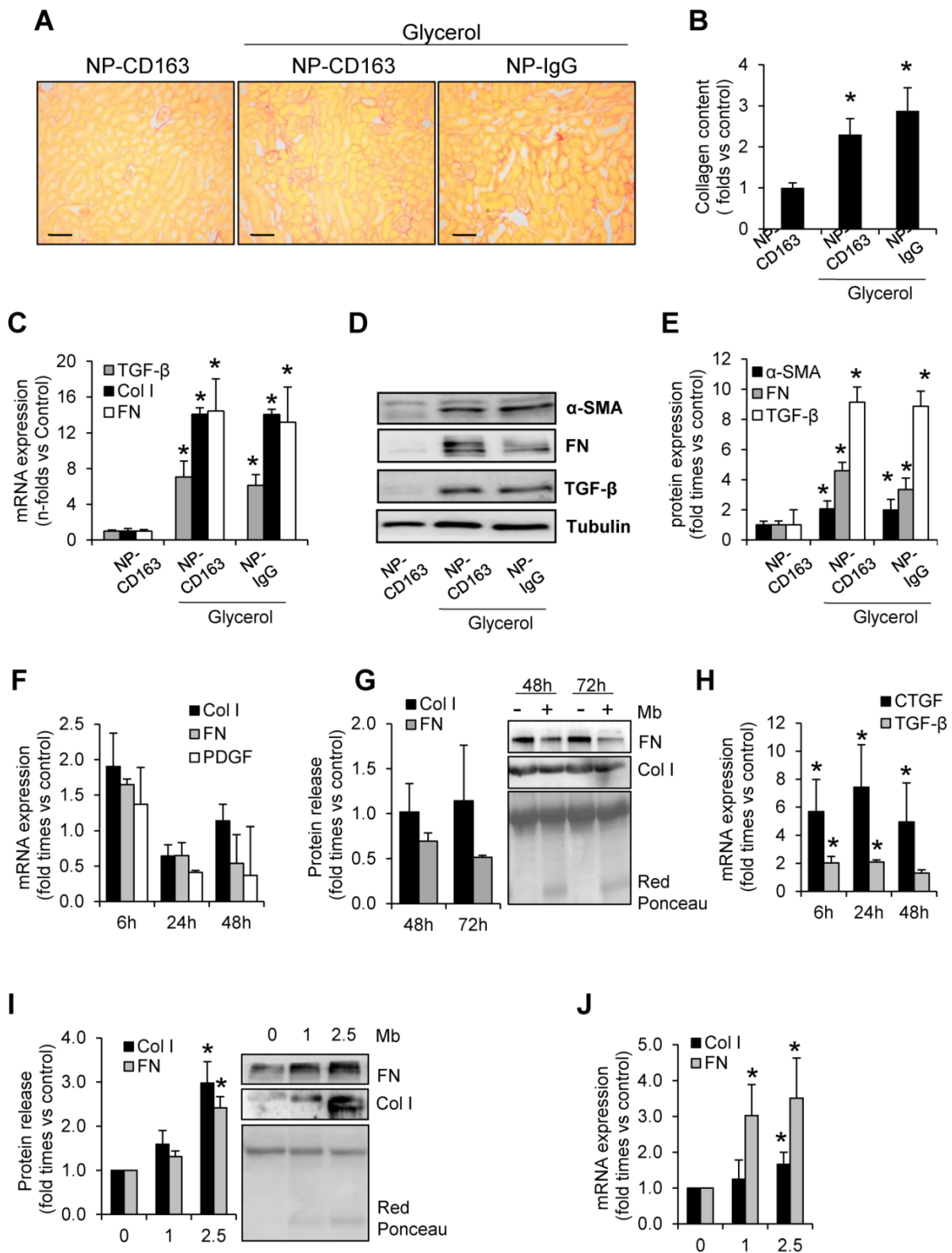
Figure 7. Rhabdomyolysis induces renal fibrosis. Representative images showing kidney collagen content by Sirius red (**A**) and semiquantitative assessment (**B**) in mice with rhabdomyolysis, scale bar 100 µM. Expression of fibronectin (FN), type I collagen (Col I), alpha smooth muscle actin (α-SMA) and the pro-fibrotic mediator transforming growth factor (TGF-β), as determined by RT-PCR (**C**) and western-blot (**D**). Protein expression values were corrected by loading control (Tubulin). Mice (n=5) per group. * p<0.05 vs non-treated mice. In other hand, to determine whether macrophages were involved in rhabdomyolysis-associated fibrosis, we analyzed the expression of fibronectin (FN), type I collagen (Col I) platelet derived growth factor (PDGF), connective tissue growth factor (CTGF) and transforming growth factor type beta (TGF-β) at mRNA level (**F, H**) or protein secretion (**G**) in supernatants from myoglobin (1mg/mL)-stimulated murine peritoneal macrophages. Murine tubular epithelial cell line (MCT) were also treated with myoglobin (1mg/mL) to determine the expression (**I**) and release (**J**) of extracellular matrix proteins (Col I and FN). Results are expressed as mean±SE of at least three independent experiments. * p<0.05 as compared with non-treated cells.

To our knowledge, this is the first study showing increased CD163 expression in kidneys from both human and experimental rhabdomyolysis-induced AKI. CD163 is a scavenger receptor expressed by alternatively activated macrophages involved in hemoglobin uptake, with important immunoregulatory properties by inducing anti-inflammatory IL-10 release and HO-1 synthesis (43). It thus seems reasonable to speculate that the increased CD163 expression might be counteracting harmful effects of myoglobin-derived heme accumulated in the kidney as consequence of skeletal muscle necrosis (44). In this line, augmented CD163 expression was observed in diseases associated with renal accumulation of hemoglobin-derived heme, such as IgA nephritis with macroscopic hematuria-AKI (14, 15), paroxysmal nocturnal hemoglobinuria (16) and warm antibody hemolytic anemia (45). However, although CD163-macrophages may resolve rhabdomyolysis kidney injury, mainly at the beginning of renal damage, when myoglobin-derived heme is accumulated in tissue, these cells might also promote the development of interstitial fibrosis at later stages. Thus, accumulation of CD163-macrophages was reported in human and experimental glomerulonephritis, correlating with interstitial fibrosis (46-48). Therefore, although M2-macrophages are known to be indispensible for short-term recovery (49), they are also involved in the development of renal fibrosis following acute kidney injury (50).

It has been demonstrated that infiltrating macrophages phenotype changes along rhabdomyolysis progression, with an increased presence of M1 inflammatory macrophages in the first days, whereas M2 reparative macrophages became most abundant at later stages (8, 49). However, the molecular mechanisms involved in the switch of M1 macrophages towards M2 macrophages are mostly unknown. We observed increased mRNA and protein expression of M1 markers (Arg2, CCL2, CCL5, TNF-α) from day 1 to 3, decreasing at day 7; whereas M2 markers (Arg-1, IL-10 and CD163) increased besides day 3. Once filtered, myoglobin is uptaken by tubular epithelial cells, promoting the release of inflammatory chemokines, thus promoting the recruitment of blood monocytes in the kidneys and a rapidly differentiation towards M1 macrophages, such as we have observed. However, our results also showed that myoglobin promotes both HO-1 and IL-10 expression, which may lead to the induction of CD163 at later times points. In support of this hypothesis, it has been previously reported that IL-10 activates CD163 in a positive feedback loop, thus promoting the differentiation toward M2

macrophages (51). In the same line, we observed that IL-10 blockade inhibited-, while activation of HO-1 enhanced myoglobin-driven CD163 upregulation. Moreover, we found a positive association between IL-10 and CD163 mRNA expression in mice kidneys with rhabdomyolysis. Another possible mechanism that could explain the increased presence of CD163-macrophages may be related to the existence of elevated levels of free heme, which may result from 1) direct renal myoglobin accumulation and further degradation or 2) from heme-containing proteins, such as cytochromes, that are commonly released as consequence of tubular cell death in rhabdomyolysis. Heme, similar to hemoglobin and erythrocytes, induces CD163 expression, such as we have observed, and it has been previously demonstrated (17). Barros et al. suggested that CD163 cannot be considered a reliable M2 marker when used on its own (52). However, in our study co-localization studies showed that CD163 was mainly expressed in macrophages that simultaneously expressed other M2 markers such as CD206 and CD163L1, corroborating a M2-skewed polarization phenotype throughout the phase of rhabdomyolysis recovery. Macrophage polarization is a dynamic process and, therefore, M1 and M2 phenotypes may be present simultaneously in the same cell (53). Therefore, we cannot exclude that anti-inflammatory CD163-macrophages, may express simultaneously M1 and M2 markers, representing plasticity of macrophage differentiation in human disease.

It is important to note that CD163 is a promising therapeutic target for selective intracellular delivery of anti-inflammatory glucocorticoids to macrophages, avoiding systemic side effects of these compounds (54, 55). Therefore, CD163 may be a new therapeutic target to modulate macrophage activity in rhabdomyolysis associated renal damage. Future studies are necessary to validate this hypothesis.

Targeting macrophages by non invasive imaging techniques may be an interesting strategy in rhabdomyolysis since these cells play an important role in this syndrome (8, 41). Specifically, the use of probes targeting CD163-macrophages by MRI may provide important information about the cellular composition of renal lesions that could be relevant for the therapeutic management of patients with rhabdomyolysis. We previously prepared gold-coated iron oxide nanoparticles linked to anti-CD163 antibodies for selective detection of M2-macrophages *in vivo* (34). In renal patients, these iron oxide nanoparticles represent an alternative to the contrast agents based on gadolinium, which promotes fibrosis and results nephrotoxic (56, 57). We noted an increased accumulation of the NP-CD163 probe in

kidneys from mice with rhabdomyolysis, whereas no signal variation was reported in healthy mice injected with NP-CD163 or in glycerol-injected mice and treated with NP-IgG, as control probe. Immunohistochemical analysis and gene expression studies confirmed the presence of CD163-positive macrophages in kidneys harvested from imaged mice with rhabdomyolysis. Likewise, electron microscopy analysis confirmed the presence of nanoparticles within interstitial macrophages exclusively in kidneys from mice with rhabdomyolysis and injected with NP-CD163. All together, our results suggest that the NP-CD163 probe may be suitable for the specific detection of M2-like macrophages in rhabdomyolysis. This diagnostic tool may be applicable not only to rhabdomyolysis, but also to other inflammatory pathologies where increased CD163-macrophage infiltration has been reported, such as cancer, rheumatoid arthritis, atherosclerosis and hemoglobin-associated renal diseases, including both haematuric glomerulonephritis and massive intravascular hemolisis (14-16).

In conclusion, our data suggest that CD163 may play an important role in the resolution of rhabdomyolysis-induced AKI in both human and mice. Myoglobin promotes an early inflammatory M1 response and a partial differentiation towards a M2-skewed polarization phenotype at later stages, where high CD163 expression is found as consequence of activation of HO-1 and IL-10 release. These myoglobin-derived macrophages may contribute to fibrosis throughout the production of fibrotic mediators, such as CTGF and TGF-β, thus contributing to the progression of rhabdomyolysis-mediated renal damage. Furthermore, our gold-coated iron oxide nanoparticles specifically detected CD163-expressing macrophages *in vivo* by MRI, providing information about the presence of M2-like macrophages in rhabdomyolysis-associated renal lesion in a non-invasive way. These CD163-grafted nanoparticles may be useful to determine macrophage subpopulations presence in other inflammatory diseases where these cells play a key role.

Material and Methods

Animal model

C57BL/6J mice (male, 12 weeks old, n=35) were purchased from Charles River Laboratories (L'Arbresle Cedex, France) and housed in a pathogen-free, temperature-controlled environment with a 12-hour/12-hour light/dark photocycle. Mice had free access to food and water. To induce rhabdomyolysis, the animals were intramuscularly injected in each thigh caudal muscle with 10 ml/kg 50% glycerol (≥99.5% m/v, G5516, Sigma, MO, USA) or saline as a control (6). Mice were dehydrated for 16 h before glycerol injection. Mice were sacrificed at 1, 3, 5 and 7 days after glycerol administration and blood, urine and kidney samples were collected. Mice were anesthetized for all procedures with isoflurane 2-3% v/v (880393, Abbott, Spain). Anesthetized mice were saline-perfused and one kidney was snap-frozen in liquid nitrogen for RNA and protein studies, and the other kidney was fixed in 4% paraformaldehyde, embedded in paraffin and used for immunohistochemistry. Blood was collected in serum tubes and stored at -80ºC until used. Serum creatinine levels were determined with a commercial assay (CRE_2c ADVIA, Siemens Healthcare, Germany) in an autoanalyzer (ADVIA® 2400 Clinical Chemistry System, Siemens Healthcare, Germany). All reported experiments were conducted in accordance with the Directive 2010/63/EU of the European Parliament and were approved by a local Institutional Animal Care and Use Committees.

Human renal biopsies

We performed a retrospective analysis of all patients hospitalized for rhabdomyolysis-AKI in both IIS-Fundación Jiménez Díaz and 12 de Octubre Hospital, Madrid, Spain. Only one kidney biopsy specimen from a patient with rhabdomyolysis-AKI was found. Control samples were obtained from non-tumor renal tissue after surgery of patients with kidney cancer. Immunohistochemical analyses were performed as further described in paraffin sections of this kidney biopsy. The patients gave informed consent and the study was approved by the local Ethics Committee.

Histopathology and immunohistochemistry.

Kidneys were cross-sectioned into 3-μm-thick pieces, dewaxed and rehydrated, and hematoxylin eosin stained. Samples were examined by an outside pathologist blinded to the nature of the samples. Tissue sections were analyzed to determine evidence of tubular damage (loss of brush border, signs of regenerations, desquamation, tubular dilation) and scored on a semiquantitative scale from 0 to 3. Results from each item were added to yield the renal injury score, which had a maximal value of 12. Renal collagen content was determined with the Sirius red staining F3BA (0.5% in saturated aqueous picric acid; 2610-10-8, Aldrich Chemical Company, MO, USA). Quantification of collagen content was performed using an image analysis system (Leica, Spain). A single investigator, unaware of the experimental groups, performed the analyses.

Immunohistochemistry and immunofluorescence studies were carried out in paraffin embedded tissue sections or cultured cells, as previously described (58). Primary antibodies were rat polyclonal anti-F4/80 antigen (1:50 dilution, MCA497G Serotec, Kidlington, UK), rabbit anti-mouse CD163 (1:50 dilution, M-96, sc-33560, Santa Cruz, Germany), rabbit anti-mouse 4-Hydroxynonenal (4-HNE) (1:100 dilution, ab46545, Abcam, Cambridge, UK), rabbit anti-mouse HO-1 (1:600 dilution, ADI-OSA-150-D, ENZO, Spain), rabbit anti-mouse CD206 (1:50 dilution, sc-48758, Santa Cruz, Germany), rabbit anti-mouse ferritin (1:800 dilution, ab86247, Abcam, Cambridge, UK). An Avidin/Biotin blocking kit (SP-2001, Vector Laboratories, Burlingame, CA, USA) was used to inhibit endogenous avidin/biotin. Negative controls using the corresponding IgG were included to check for non-specific staining. Biotinylated secondary antibodies were applied for 1 h. Then avidin–biotin peroxidase complex (Vectastain ABC kit, PK-7200, Vector Laboratories, Burlingame, CA, USA) was added for 30 min. Sections were stained with 3,3'-diaminobenzidine or 3-amino-9-ethyl carbazol (S1967, DAKO, Glostrup, Denmark), counterstained with haematoxylin. Sections were counterstained with Carazzi's hematoxylin. For CD163 detection in mouse kidneys, Tyramide Signal Amplification Biotin Kit (NEL700A001KT, PerkinElmer, MA, USA) was needed to improve signal detection. Images were taken using a Nikon Eclipse E400 microscope (Japan) and Nikon ACT-1 software (Japan). Quantification of F4/80 and CD163 positive-stained cells was made by determining the total number of positive cells/total number of cells in 20 randomly chosen fields (x100) using Image-Pro Plus software (Media Cybernetics, Rockville, MD, USA). For immunofluorescence studies, murine peritoneal macrophages were plated onto Labtek slides, fixed in 4% paraformaldehyde and permeabilized in 0.2% Triton X-100/PBS, washed in PBS, and incubated with rabbit anti-mouse HO-1 (1:200 dilution, ADI-OSA-150-D, ENZO, Spain), followed by Alexa 488 secondary antibody (1:200, A11090, Invitrogen, Eugene, OR, USA). Paraffin embedded tissue sections were incubated with mouse anti-human CD68 (1:100 dilution; A-21052, Dako ,Glostrup, Denmark), rabbit anti-human CD163L1 (1:100 dilution, HPA015663, Sigma-Aldrich, St. Louis, MO, USA), rabbit anti-human CD206 (1:100 dilution, sc-48758, Santa Cruz, Germany) and rabbit anti-human CD163 (1:100 dilution; AM21062PU-N, ACRIS, Germany) followed by Alexa 488 or Alexa 633 as secondary antibodies, respectively (1:200, A-11001 and A-21070, respectively, Invitrogen, Eugene, OR, USA) and analyzed in a confocal microscope (SPE; Leica Microsystems, Buffalo Grove, IL, USA). Nuclei were counterstained with 4'-6-diamidino-2-phenylindole (DAPI). Quantification of protein expression (as relative fluorescence intensity [RFI] within regions of interest) was performed in 10 random fields (×40)/sample with the ImageJ software (National Institutes of Health, Bethesda, MD, USA) using similar acquisition settings in all tissues. CD163L1$^+$and CD206$^+$ RFI values were calculated from CD163+ macrophages segmented with the ImageJ software. Cells were considered positive for a marker when the RFI was > 25 arbitrary units (A.U.). After background subtraction, the data were plotted using the Prism, version 5.0, software (GraphPad Software, San Diego, CA, USA).

TUNEL assay

The degree of apoptosis was assessed using a TUNEL assay. Detection of DNA fragmentation was performed using a kit from Roche Applied Sciences (06432344001, Indianapolis, IN, USA). A semiquantitative analysis was performed by counting the number of TUNEL-positive cells per field in the renal tissue at ×400 magnification. At least 10 areas in the cortex per slide were randomly selected. The mean number of green colored cells in these selected fields was expressed as the number of TUNEL-positive cells.

Cell Culture

Proximal tubular epithelial MCT cells were cultured in RPMI 1640 (R0883, Sigma, MO, USA) supplemented with decomplemented fetal bovine serum (FBS) (10%) (F7524, Sigma, MO, USA), glutamine (2 mmol/l) (G7513, Sigma, MO, USA), and penicillin/streptomycin (100 U/ml; P0781, Sigma, MO, USA) in 5% CO_2 at 37 °C. Murine peritoneal macrophages were isolated and cultured as previously described (59). MCT and murine macrophages were stimulated with myoglobin (0-2.5 mg/mL) (M1882, Sigma, MO, USA) to determine the expression of pro-inflammatory cytokines, several M1/M2 macrophage markers and fibrotic molecules. Heme (60µM; 16003-13-5, Sigma, MO, USA), HO-1 inducer CoPP (Cobalt protoporphyrin) (3µM, Co654-9, Frontier Scientific, USA) and an IL-10 blocking antibody (1µg/mL) (AF519, R&D, Canada) were used to analyze CD163 expression in mouse peritoneal macrophages.

ELISA

Concentrations of murine IL-10 (EM2IL10, Thermo Scientific, USA) in the supernatants of the cell cultures were determined by ELISA, following the manufacturer's instructions.

RNA Extraction and real-time PCR

Total RNA from kidneys or cultured cells was obtained by Trizol method (10296-028, Invitrogen, Carlsbad, CA, USA) and reverse-transcribed with High Capacity cDNA Archive Kit and real-time PCR was performed on a ABI Prism 7500 PCR system (Applied Biosystems, Foster City, CA, USA) using the DeltaDelta Ct method. Expression levels are given as ratios to Glyceraldehyde 3-phosphate dehydrogenase (GADPH). Expression of target genes was analyzed by real-time quantitative PCR using Tagman ® gene expression assays for murine GADPH (Mm99999915_g1), Kim-1 (Mm00506686_m1), CCL2 (Mm00441242_m1), CCL5 (Mm01302428_m1), IFN-γ (Mm01168134_m1), TNF-α (Mm00443258_m1) , IL-4 (Mm01275139_m1), IL-10 (Mm00439614_m1), IL-12 (Mm00434169_m1), HO-1 (Mm00516005_m1), Collagen type I (Mm00801666_g1), Fibronectin (Mm01256744_m1), platelet derived growth factor (PDGF) (Mm00546829_m1), transforming growth factor-beta (TGF-β) (Mm01178819_m1), α-smooth muscle actin (α-SMA) (Mm00725412_s1) (Applied Biosystems, Foster City, CA, USA) and designed probes for Arg1 (forward-5´-TTAGGGTTACGGCCG GTGGAGAGGA-3´, reverse-5´-TGCTGCATGTGCTC GGGCTGT-3´) and Arg2 (forward 5´-TTGGCCTGAG AGATGTGGAGCCTCC-3´, reverse 5´-ACTCAGGTG GATTGGCCTCTGCC-3´) (Fisher Scientific, Spain).

Western blot

Tissue samples were homogenized in lysis buffer (50mM TrisHCl, 150mM NaCl, 2 mM EDTA, 2 mM EGTA, 0.2% Triton X-100, 0.3% NP-40, 0.1 mM PMSF, and 1 µg/ml pepstatin A) and then separated by 10% SDS-PAGE under reducing conditions. After electrophoresis, samples were transferred to PVDF membranes (IPVH00010, Millipore, Bedford, MA, USA), blocked with 5% skimmed milk in TBS/0.5% v/v Tween 20 for 1 h, washed with TBS/Tween, and incubated with rabbit anti-Fibronectin (1:5000; AB2033, Millipore, MA, USA), anti-alpha smooth muscle actin (α-SMA) (1:1000; A2668, Sigma, MO, USA), anti-Collagen I (1:1000, 234167, Merck Millipore, MA, USA), anti-Arg1 (1:1000; sc-20150, Santa Cruz, Germany), anti-Arg2 (1:1000; sc-393496, Santa Cruz, Germany). Antibodies were diluted in 5% milk TBS/Tween. Blots were washed with TBS/Tween and incubated with appropriate horseradish peroxidase-conjugated secondary antibody (1:2000, Amersham, Aylesbury, UK). After washing with TBS/Tween the blots were developed with the chemiluminescence method (ECL Luminata Crescendo, WBLUR0500, Millipore, MA, USA). Blots were then probed with mouse monoclonal anti-α-tubulin antibody (1:5000, T6199, Sigma, MO,

USA), and levels of expression were corrected for minor differences in loading. Quantification was expressed as arbitrary densitometric units (AU).

Synthesis of gold-coated iron oxide nanoparticles and functionalization with IgG antibodies.

Water soluble gold coated iron oxide nanoparticles were prepared as previously described (31, 34). First, hexane soluble oleic acid protected gold coated iron oxide nanoparticles (Fe_3O_4@Au@oleic NPs) were prepared from iron oxide seeds following a modification of a procedure reported by Wang *et al.* (60). Such oleic acid protected gold-coated iron oxide nanoparticles (Fe_3O_4@Au@oleic NPs) underwent a ligand exchange step with a 1:1 mixture of carboxylic acid ending ligands and mannose ending ligands to yield water soluble Fe_3O_4@Au nanoparticles (Fe_3O_4@Au@Man/CO_2H NPs). These nanoparticles were characterized by TEM on a JEOL JEM 2100F microscope (Japan), Cary UV-Vis spectrophotometer (Agilent, USA) and ICP-OES (Inductively coupled plasma-optical emission spectroscopy, 700 ICP-OES, Agilent Technologies, CA, USA) for the quantification of the gold and iron content. Subsequently, water soluble Fe_3O_4@Au@Man/CO_2H NPs were converted into targeted NPs through a peptide coupling with amine groups present in protein G (Pierce™ Recombinant Protein G, (Catalog number: 21193, Thermo Scientific, Belgium) and further incubation of IgG antibodies with the NP-protG complex, following a two-step procedure described in the literature for the same nanoparticles (33).

Mouse anti-CD163 (M-96, sc-33560, Santa Cruz, Germany) and IgG isotype antibody (sc-2027, Santa Cruz, Germany) were conjugated to the NP-protG complex leading to the formation of 2 probes: NP-CD163 and NP-IgG for anti-CD163 and IgG antibodies, respectively. The amount of protG and antibody on the nanoparticles was separately determined by Bradford assay of the unbound protG or the antibody recovered in the washings after the peptide coupling or the antibody incubation, as previously described (33). The amount of protG-IgG complex on each nanoparticle ranged from 1 to 2 units.

In vitro validation of the gold-coated iron oxide nanoparticles functionalized with antibodies against CD163 by MRI

Murine peritoneal macrophages ($5x10^5$ cells) were treated for 24 h with dexamethasone (2.5×10^{-7} M) to induce CD163 expression, as previously reported (61). Murine macrophages, expressing or not CD163, were incubated with either

NP-CD163 or NP-IgG (as control) at 4 °C, employing 0.75 µg of Fe per 5×10^5 cells in 300 µL of PBS. After 1 hour the cells were centrifuged to remove the unbound NPs and several washings with PBS were performed. The incubated cells were placed in capillary tubes and allowed to form a pellet overnight at 4°C. Capillary tubes were then inserted in agarose gel (2% w/w) to prepare phantoms for MRI. T_2 relaxation times for each pellet were calculated from images obtained using a multiple spin echo sequence with equally spaced 64 echoes ranging from 10 ms to 640 ms and 12000 ms repetition time. The in plane resolution was 133×133 μm^2 and the slice thickness varied between 300 µm and 500 µm in the different samples. The slice thickness was varied to avoid partial volume effects from the water above the pellet of cells, as the volume of pellet could vary from sample to sample. Each echo was acquired 8 times to improve the signal to noise ratio.

Imaging of mice

Nanoparticles (2mg Fe/Kg mice) were injected intravenously via retro-orbital 3 days after glycerol/saline injection. Images of the same mice were acquired before nanoparticles injection and 48 hours after nanoparticles injection. Imaging studies were carried out on a small animal horizontal 7 Tesla (T) Bruker Biospec 70/30 magnet (Ettlingen, Germany), B-GA12 gradient coil insert and 40 mm inner diameter transmit-receive volume coil. Before imaging, mice were anesthetized with isoflurane (1.5% in O_2) and positioned supine, with the kidneys placed at the center of the NMR coil. The breathing rate was monitored using an air balloon placed on top of the chest (SA Instruments, Inc., NY, USA). The respiration rates were similar for every experiment. T_2-weighted images were acquired using Rapid Acquisition with Relaxation Enhancement (RARE) acquisition method applied with an effective TE of 36 ms (RARE factor 4), TR 2000 ms; field-of-view of 30x30 mm at 256x256 matrix, and 40 kHz effective spectral bandwidth; 6 averages; 15 contiguous axial slices of 1 mm thickness.

MRI images were analyzed using Image J (Image J 1.44p, NIH, USA) and regions of interest were manually segmented to determine their signal-to-noise-ratio (SNR), which was defined as: $SNR_{ROI} = I_{ROI}/SD_{NOISE}$. Where I_{ROI} is the intensity either in kidney cortex or in muscle and SD_{NOISE} is the standard deviation outside the mouse. The normalized-enhancement-ratio of the kidney cortex (NER_c) 48 hours after injection with respect to muscle was defined as: $NER_c = (SNR_c/SNR_m)_{post}/(SNR_c/SNR_m)_{pre}$ x 100 (%). The contrast-to-noise-ratio of the kidney cortex (CNR_c)

with respect to the muscle was also calculated and defined as: $CNR_c = SNR_c-SNR_m$. After imaging studies, anesthetized mice were saline-perfused and one kidney was snap-frozen in liquid nitrogen for RNA and protein studies, a small piece of renal cortex of the other kidney was fixed for transmission electron microscopy and the remaining kidney was fixed in 4% paraformaldehyde, embedded in paraffin and used for immunohistochemistry. Blood was collected in serum tubes and stored at -80ºC until used.

Transmission electron microscopy of renal tissue samples

A portion of renal cortex was fixed with 1% glutaraldehyde and 4% formaldehyde in PBS and stored at 4°C. The kidneys were then postfixed in a solution of 1% OsO_4 in H_2O for 1 hour, dehydrated with ethanol (30-100%) and acetone (100%), and embedded in Durcupan resin. Ultrathin sections (50–90 nm) were then stained with a solution of 2% uranyl acetate in H_2O for 20 min. The preparations were examined with a JEOL JEM1010 transmission electron microscope (Tokyo, Japan) at 80 Kv.

Statistics

Data are expressed as means ± SD. Data comparisons between experimental groups at each time point were analyzed with the Kruskall-Wallis test and the Mann-Whitney U-test. P values <0.05 were considered significant. Statistical analysis was performed using SPSS 11.0 statistical software.

Supplementary Material

Supplementary tables and figures.
http://www.thno.org/v06p0896s1.pdf

Acknowledgements

Competing Interests

References

1. Bosch X, Poch E, Grau JM. Rhabdomyolysis and acute kidney injury. N Engl J Med 2009;361:62-72.
2. Melli G, Chaudhry V, Cornblath DR. Rhabdomyolysis: an evaluation of 475 hospitalized patients. Medicine (Baltimore) 2005;84:377-85.
3. Bagley WH, Yang H, Shah KH. Rhabdomyolysis. Intern Emerg Med 2007;2:210-8.
4. Kim JH, Lee SS, Jung MH, Yeo HD, Kim HJ, Yang JI, et al. N-acetylcysteine attenuates glycerol-induced acute kidney injury by regulating MAPKs and Bcl-2 family proteins. Nephrol Dial Transplant 2010;25:1435-43.
5. Homsi E, Janino P, de Faria JB. Role of caspases on cell death, inflammation, and cell cycle in glycerol-induced acute renal failure. Kidney Int 2006;69:1385-92.
6. Wei Q, Hill WD, Su Y, Huang S, Dong Z. Heme oxygenase-1 induction contributes to renoprotection by G-CSF during rhabdomyolysis-associated acute kidney injury. Am J Physiol Renal Physiol 2011;301:F162-F170.
7. Kim JH, Lee DW, Jung MH, Cho HS, Jeon DH, Chang SH, et al. Macrophage depletion ameliorates glycerol-induced acute kidney injury in mice. Nephron Exp Nephrol 2014;128:21-9.
8. Belliere J, Casemayou A, Ducasse L, Zakaroff-Girard A, Martins F, Iacovoni JS, et al. Specific macrophage subtypes influence the progression of rhabdomyolysis-induced kidney injury. J Am Soc Nephrol 2015;26:1363-77.
9. Anders HJ, Ryu M. Renal microenvironments and macrophage phenotypes determine progression or resolution of renal inflammation and fibrosis. Kidney Int 2011;80:915-25.
10. Nelson PJ, Rees AJ, Griffin MD, Hughes J, Kurts C, Duffield J. The renal mononuclear phagocytic system. J Am Soc Nephrol 2012;23:194-203.
11. Philippidis P, Mason JC, Evans BJ, Nadra I, Taylor KM, Haskard DO, et al. Hemoglobin scavenger receptor CD163 mediates interleukin-10 release and heme oxygenase-1 synthesis: antiinflammatory monocyte-macrophage responses in vitro, in resolving skin blisters in vivo, and after cardiopulmonary bypass surgery. Circ Res 2004;94:119-26.
12. Stocker R. Induction of haem oxygenase as a defence against oxidative stress. Free Radic Res Commun 1990;9:101-12.
13. Moreno JA, Martin-Cleary C, Gutierrez E, Toldos O, Blanco-Colio LM, Praga M, et al. AKI associated with macroscopic glomerular hematuria: clinical and pathophysiologic consequences. Clin J Am Soc Nephrol 2012;7:175-84.
14. Martin CC, Moreno JA, Fernandez B, Ortiz A, Parra EG, Gracia C, et al. Glomerular haematuria, renal interstitial haemorrhage and acute kidney injury. Nephrol Dial Transplant 2010;25:4103-6.
15. Gutierrez E, Egido J, Rubio-Navarro A, Buendia I, Blanco Colio LM, Toldos O, et al. Oxidative stress, macrophage infiltration and CD163 expression are determinants of long-term renal outcome in macrohematuria-induced acute kidney injury of IgA nephropathy. Nephron Clin Pract 2012;121:c42-c53.
16. Ballarin J, Arce Y, Torra BR, Diaz EM, Manzarbeitia F, Ortiz A, et al. Acute renal failure associated to paroxysmal nocturnal haemoglobinuria leads to intratubular haemosiderin accumulation and CD163 expression. Nephrol Dial Transplant 2011;26:3408-11.
17. Boyle JJ, Johns M, Lo J, Chiodini A, Ambrose N, Evans PC, et al. Heme induces heme oxygenase 1 via Nrf2: role in the homeostatic macrophage response to intraplaque hemorrhage. Arterioscler Thromb Vasc Biol 2011;31:2685-91.
18. Temme S, Bonner F, Schrader J, Flogel U. 19F magnetic resonance imaging of endogenous macrophages in inflammation. Wiley Interdiscip Rev Nanomed Nanobiotechnol 2012;4:329-43.
19. Weissleder R, Nahrendorf M, Pittet MJ. Imaging macrophages with nanoparticles. Nat Mater 2014;13:125-38.
20. Korchinski DJ, Taha M, Yang R, Nathoo N, Dunn JF. Iron Oxide as an MRI Contrast Agent for Cell Tracking. Magn Reson Insights 2015;8:15-29.
21. Beckmann N, Cannet C, Babin AL, Ble FX, Zurbruegg S, Kneuer R, et al. In vivo visualization of macrophage infiltration and activity in inflammation using magnetic resonance imaging. Wiley Interdiscip Rev Nanomed Nanobiotechnol 2009;1:272-98.
22. Alam SR, Tse GH, Stirrat C, MacGillivray TJ, Lennen RJ, Jansen MA, et al. Nanoparticle enhanced MRI scanning to detect cellular inflammation in experimental chronic renal allograft rejection. Int J Mol Imaging 2015;2015:507909.
23. Chae EY, Song EJ, Sohn JY, Kim ST, Woo CW, Gong G, et al. Allogeneic renal graft rejection in a rat model: in vivo MR imaging of the homing trait of macrophages. Radiology 2010;256:847-54.
24. Beckmann N, Cannet C, Zurbruegg S, Haberthur R, Li J, Pally C, et al. Macrophage infiltration detected at MR imaging in rat kidney allografts: early marker of chronic rejection? Radiology 2006;240:717-24.
25. Egger C, Cannet C, Gerard C, Debon C, Stohler N, Dunbar A, et al. Adriamycin-induced nephropathy in rats: functional and cellular effects characterized by MRI. J Magn Reson Imaging 2015;41:829-40.
26. Cai QY, Lee H, Kim EJ, Moon H, Chang K, Rho J, et al. Magnetic resonance imaging of superparamagnetic iron oxide-labeled macrophage infiltrates in acute-phase renal ischemia-reperfusion mouse model. Nanomedicine 2012;8:365-73.
27. Al FA, Luciani N, Kolosnjaj-Tabi J, Mattar E, Clement O, Wilhelm C, et al. Real-time high-resolution magnetic resonance tracking of macrophage subpopulations in a murine inflammation model: a pilot study with a commercially available cryogenic probe. Contrast Media Mol Imaging 2013;8:193-203.
28. Mikita J, Dubourdieu-Cassagno N, Deloire MS, Vekris A, Biran M, Raffard G, et al. Altered M1/M2 activation patterns of monocytes in severe relapsing experimental rat model of multiple sclerosis. Amelioration of clinical status by M2 activated monocyte administration. Mult Scler 2011;17:2-15.
29. Moller HJ. Soluble CD163. Scand J Clin Lab Invest 2012;72:1-13.
30. Estelrich J, Sanchez-Martin MJ, Busquets MA. Nanoparticles in magnetic resonance imaging: from simple to dual contrast agents. Int J Nanomedicine 2015;10:1727-41.
31. Gallo J, Garcia I, Genicio N, Padro D, Penades S. Specific labelling of cell populations in blood with targeted immuno-fluorescent/magnetic glyconanoparticles. Biomaterials 2011;32:9818-25.
32. Elvira G, Garcia I, Benito M, Gallo J, Desco M, Penades S, et al. Live imaging of mouse endogenous neural progenitors migrating in response to an induced tumor. PLoS One 2012;7:e44466.
33. Garcia I, Gallo J, Genicio N, Padro D, Penades S. Magnetic glyconanoparticles as a versatile platform for selective immunolabeling and imaging of cells. Bioconjug Chem 2011;22:264-73.
34. Tarin C, Carril M, Martin-Ventura JL, Markuerkiaga I, Padro D, Llamas-Granda P, et al. Targeted gold-coated iron oxide nanoparticles for CD163 detection in atherosclerosis by MRI. Sci Rep 2015;5:17135.
35. Nath KA, Haggard JJ, Croatt AJ, Grande JP, Poss KD, Alam J. The indispensability of heme oxygenase-1 in protecting against acute heme protein-induced toxicity in vivo. Am J Pathol 2000;156:1527-35.
36. Sierra-Filardi E, Vega MA, Sanchez-Mateos P, Corbi AL, Puig-Kroger A. Heme Oxygenase-1 expression in M-CSF-polarized M2 macrophages contributes to LPS-induced IL-10 release. Immunobiology 2010;215:788-95.
37. Moreno JA, Ortega-Gomez A, Delbosc S, Beaufort N, Sorbets E, Louedec L, et al. In vitro and in vivo evidence for the role of elastase shedding of CD163 in human atherothrombosis. Eur Heart J 2012;33:252-63.
38. Sinniah R, Lye W. Acute renal failure from myoglobinuria secondary to myositis from severe falciparum malaria. Am J Nephrol 2000;20:339-43.
39. Ayer G, Grandchamp A, Wyler T, Truniger B. Intrarenal hemodynamics in glycerol-induced myohemoglobinuric acute renal failure in the rat. Circ Res 1971;29:128-35.
40. Kurtz TW, Maletz RM, Hsu CH. Renal cortical blood flow in glycerol-induced acute renal failure in the rat. Circ Res 1976;38:30-5.
41. Kim JH, Lee DW, Jung MH, Cho HS, Jeon DH, Chang SH, et al. Macrophage depletion ameliorates glycerol-induced acute kidney injury in mice. Nephron Exp Nephrol 2014;128:21-9.
42. Venkatachalam MA, Weinberg JM, Kriz W, Bidani AK. Failed Tubule Recovery, AKI-CKD Transition, and Kidney Disease Progression. J Am Soc Nephrol 2015;26:1765-76.
43. Philippidis P, Mason JC, Evans BJ, Nadra I, Taylor KM, Haskard DO, et al. Hemoglobin scavenger receptor CD163 mediates interleukin-10 release and heme oxygenase-1 synthesis: antiinflammatory monocyte-macrophage responses in vitro, in resolving skin blisters in vivo, and after cardiopulmonary bypass surgery. Circ Res 2004;94:119-26.
44. Herrera MB, Bussolati B, Bruno S, Fonsato V, Romanazzi GM, Camussi G. Mesenchymal stem cells contribute to the renal repair of acute tubular epithelial injury. Int J Mol Med 2004;14:1035-41.
45. Fervenza FC, Croatt AJ, Bittar CM, Rosenthal DW, Lager DJ, Leung N, et al. Induction of heme oxygenase-1 and ferritin in the kidney in warm antibody hemolytic anemia. Am J Kidney Dis 2008;52:972-7.
46. Ikezumi Y, Suzuki T, Karasawa T, Hasegawa H, Yamada T, Imai N, et al. Identification of alternatively activated macrophages in new-onset paediatric and adult immunoglobulin A nephropathy: potential role in mesangial matrix expansion. Histopathology 2011;58:198-210.
47. Ikezumi Y, Suzuki T, Karasawa T, Hasegawa H, Kawachi H, Nikolic-Paterson DJ, et al. Contrasting effects of steroids and mizoribine on macrophage activation and glomerular lesions in rat thy-1 mesangial proliferative glomerulonephritis. Am J Nephrol 2010;31:273-82.
48. Han Y, Ma FY, Tesch GH, Manthey CL, Nikolic-Paterson DJ. Role of macrophages in the fibrotic phase of rat crescentic glomerulonephritis. Am J Physiol Renal Physiol 2013;304:F1043-F1053.
49. Geng Y, Zhang L, Fu B, Zhang J, Hong Q, Hu J, et al. Mesenchymal stem cells ameliorate rhabdomyolysis-induced acute kidney injury via the activation of M2 macrophages. Stem Cell Res Ther 2014;5:80.
50. Kim MG, Kim SC, Ko YS, Lee HY, Jo SK, Cho W. The Role of M2 Macrophages in the Progression of Chronic Kidney Disease following Acute Kidney Injury. PLoS One 2015;10:e0143961.
51. Boyle JJ, Harrington HA, Piper E, Elderfield K, Stark J, Landis RC, et al. Coronary intraplaque hemorrhage evokes a novel atheroprotective macrophage phenotype. Am J Pathol 2009;174:1097-108.
52. Barros MH, Hauck F, Dreyer JH, Kempkes B, Niedobitek G. Macrophage polarisation: an immunohistochemical approach for identifying M1 and M2 macrophages. PLoS One 2013;8:e80908.
53. Martinez FO, Gordon S. The M1 and M2 paradigm of macrophage activation: time for reassessment. F1000Prime Rep 2014;6:13.

54. Granfeldt A, Hvas CL, Graversen JH, Christensen PA, Petersen MD, Anton G, et al. Targeting dexamethasone to macrophages in a porcine endotoxemic model. Crit Care Med 2013;41:e309-e318.

55. Graversen JH, Svendsen P, Dagnaes-Hansen F, Dal J, Anton G, Etzerodt A, et al. Targeting the hemoglobin scavenger receptor CD163 in macrophages highly increases the anti-inflammatory potency of dexamethasone. Mol Ther 2012;20:1550-8.

56. Canavese C, Mereu MC, Aime S, Lazzarich E, Fenoglio R, Quaglia M, et al. Gadolinium-associated nephrogenic systemic fibrosis: the need for nephrologists' awareness. J Nephrol 2008;21:324-36.

57. Kay J. Nephrogenic systemic fibrosis: a gadolinium-associated fibrosing disorder in patients with renal dysfunction. Ann Rheum Dis 2008;67 Suppl 3:iii66-iii69.

58. Moreno JA, Izquierdo MC, Sanchez-Nino MD, Suarez-Alvarez B, Lopez-Larrea C, Jakubowski A, et al. The inflammatory cytokines TWEAK and TNFalpha reduce renal klotho expression through NFkappaB. J Am Soc Nephrol 2011;22:1315-25.

59. Mallavia B, Oguiza A, Lopez-Franco O, Recio C, Ortiz-Munoz G, Lazaro I, et al. Gene Deficiency in Activating Fcgamma Receptors Influences the Macrophage Phenotypic Balance and Reduces Atherosclerosis in Mice. PLoS One 2013;8:e66754.

60. Wang L, Luo J, Fan Q, Suzuki M, Suzuki IS, Engelhard MH, et al. Monodispersed core-shell Fe3O4@Au nanoparticles. J Phys Chem B 2005;109:21593-601.

61. Moreno JA, Munoz-Garcia B, Martin-Ventura JL, Madrigal-Matute J, Orbe J, Paramo JA, et al. The CD163-expressing macrophages recognize and internalize TWEAK: potential consequences in atherosclerosis. Atherosclerosis 2009;207:103-10.